Journal of composites science

MDPI

Article

Spray-Dried Cellulose Nanofibril-Reinforced Polypropylene Composites for Extrusion-Based Additive Manufacturing: Nonisothermal Crystallization Kinetics and Thermal Expansion

Lu Wang [1,2,*], William M. Gramlich [3], Douglas J. Gardner [1,2], Yousoo Han [1,2] and Mehdi Tajvidi [1,2]

1 Advanced Structures and Composites Center, University of Maine, 35 Flagstaff Road, Orono, ME 04469-5793, USA; douglasg@maine.edu (D.J.G.); yousoo.han@maine.edu (Y.H.); mehdi.tajvidi@maine.edu (M.T.)
2 School of Forest Resources, University of Maine, 5755 Nutting Hall, Orono, ME 04469-5755, USA
3 Department of Chemistry, University of Maine, 171 Aubert Hall, Orono, ME 04469, USA; william.gramlich@maine.edu
* Correspondence: lu.wang@maine.edu; Tel.: +1-207-581-2402; Fax: +1-207-581-2074

Received: 17 January 2018; Accepted: 7 February 2018; Published: 9 February 2018

Abstract: Isotactic polypropylene (iPP) is a versatile polymer. It accounts for the second-largest polymer consumption worldwide. However, iPP is difficult to 3D print via extrusion-based processing. This is attributable to its rapid crystallization rate. In this study, spray-dried cellulose nanofibrils (SDCNF) and maleic anhydride polypropylene (MAPP) were investigated to reveal their effects on the nonisothermal crystallization kinetics and thermal expansion of iPP. SDCNF at 3 wt % and 30 wt % accelerated the crystallization rate of iPP, while SDCNF at 10 wt % retarded the crystallization rate by restricting crystal growth and moderately increasing the nucleation density of iPP. Additionally, adding MAPP into iPP/SDCNF composites accelerated the crystallization rate of iPP. The effective activation energy of iPP increased when more than 10 wt % SDCNF was added. Scanning electron microscopy and polarized light microscopy results indicated that high SDCNF content led to a reduced gap size among SDCNF, which hindered the iPP crystal growth. The coefficient of thermal expansion of iPP/SDCNF10% was 11.7% lower than the neat iPP. In summary, SDCNF, at 10 wt %, can be used to reduce the warping of iPP during extrusion-based additive manufacturing.

Keywords: additive manufacturing; fused deposition modeling; 3D printing; polypropylene; crystallization retardant; transcrystallization; nucleation

1. Introduction

Cellulose nanofibrils (CNF) are a type of cellulose nanofiber which are derived from wood pulp by mechanical disintegration [1]. CNF was found to be a good mechanical reinforcement for polymers because of its high stiffness and fibril-like structure [2]. For the direct incorporation of CNF into a hydrophobic thermoplastic matrix by conventional manufacturing methods, it is preferable that the fiber is in dried form: this facilitates the processing stage [3]. Spray drying was reported to be a good way of obtaining dried CNF in terms of drying costs and industrial scalability [3]. Extrusion-based additive manufacturing (EAM) is one of the additive manufacturing methods that can be used to print thermoplastics. Because of its low cost and simple operation, EAM is the most popular 3D printing technique. However, EAM cannot print all thermoplastic polymers, for example, isotactic polypropylene (iPP) [4]. Because iPP crystallizes quickly, the printed layers shrink and warp during the deposition of subsequent layers. Table 1 displays a comparison on the crystallization rate of iPP and poly(L-lactide) (PLLA) [5,6]. Because PLLA crystallizes much more slowly than iPP under the

same processing conditions, PLLA is easier to use in the EAM process. Because iPP a very versatile material with worldwide consumption, addressing its issue in 3D printing is important. To use iPP in the EAM process, retarding the crystallization rate is required.

Table 1. A comparison on the crystallization rate of iPP and PLLA.

Materials	M_n [a] (g/mol)	T_c [b] (°C)	$t_{1/2}$ [c] (min)
iPP	4.18×10^4	120	2.93
PLLA	4.5×10^4	120	21.5

[a] number-based molecular weight; [b] crystallization temperature; [c] crystallization half time.

During the EAM process, the crystallization temperature profile at the center of the bottom layer of a specimen is shown in Figure 1 [7]. The printing orientation is along its long axis. The time period within that increase-decrease cycle of temperature corresponds to the time required to build each layer. The real-time temperature of one spot changes drastically when the printing nozzle is close enough to it. When the printing nozzle moves away that spot, the temperature change is small. The average temperature variation is also small. Therefore, two types of nonisothermal crystallization occur during the EAM process. One is the crystallization at high cooling rate (>20 °C/min), which only occurs when the nozzle is close enough to the polymer. This accounts for a very small portion of the crystallization process. The other one is the crystallization occurring at low cooling rate (5~10 °C/min). When the temperature drops below the crystallization temperature (T_c) of the polymer, the shrinkage of the polymer is controlled by the thermal expansion of the amorphous portion. A previous study revealed that the shrinkage of iPP above the T_c is much larger than the shrinkage below T_c when iPP is cooled from its melt state [8]. Therefore, the crystallization is the primary force that drives iPP to shrink. During the EAM processing, a bench-scale 3D printer (no screw in the barrel) induces extensional flow and large-scale 3D printers (screw in the barrel) cause shear flow. Flow-induced crystallization is an important factor which had been studied [9,10]. However, in this paper, differential scanning calorimentry (DSC) was applied to materials at quiescent state for studying the crystallization kinetics for simplicity.

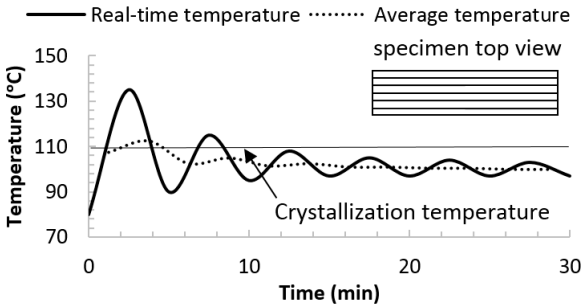

Figure 1. Cooling temperature profile of the bottom strand during extrusion-based additive manufacturing (Adapted from Sun [7]).

The addition of a higher amount (~10 wt %) of nanofillers in polymer systems was found to decrease the crystallization rate [11–13]. After drying, the SDCNF exhibits a circle-equivalent diameter of approximately 10 µm. Moreover, the majority of SDCNF particles exhibit a spherical structure with a small aspect ratio and smooth surface [14,15]. Those morphological properties can diminish the nucleation ability of CNF. Because of losing its nano-scale, a larger amount of SDCNF is needed to decelerate the overall crystallization rate of iPP as compare to CNF.

The addition of natural fibers into the iPP matrix is frequently reported to accelerate the crystallization of iPP in nonisothermal conditions by increasing the nucleation density [16–19].

The effect of surface treatments on the crystallization kinetics of iPP depends on the type of treatment [20,21]. Thermal expansion of iPP or PP/PE blends was found to decrease with increasing cellulose content [22,23]. So far, how SDCNF affects the nonisothermal crystallization kinetics and thermal expansion of iPP has not been studied. This experiment was primarily designed to analyze the effect of SDCNF content and MAPP on the nonisothermal crystallization kinetics of iPP at four cooling rates (5, 10, 15, 20 °C/min). The cooling rates were chosen based on the previous analysis of the crystallization temperature during 3D printing as shown in Figure 1. Thermal expansion analysis was performed on the group with the slowest crystallization rate. The results of this study can be helpful towards addressing the cause of iPP warping during EAM, as well as provide useful information on processing iPP/SDCNF composites via conventional methods.

2. Materials and Methods

2.1. Materials

Isotactic polypropylene (iPP) homopolymer (H19G-01) was obtained from Ineos Olefins & Polymers USA (League City, TX, USA). The iPP grade is specified for the extrusion of continuous filaments. Basic iPP material properties are a density of 0.91 g/cm^3, melting point of 160 °C, melt flow index of 19 g/10 min (230 °C/2.16 kg), tensile strength (yield) of 37.2 MPa, flexural modulus of 1.78 GPa and notched Izod impact Strength of 2.8 kJ/m^2. Maleic anhydride polypropylene (MAPP) pellets (Polybond 3200) with a maleic anhydride content of about 1.0 wt % were obtained from Chemtura Corporation (Lawrenceville, GA, USA). The MAPP has a density of 0.91 g/cm^3 and a MFI of 115 g/10 min (190 °C/2.16 kg). Cellulose nanofibrils suspension (~3 wt %) was obtained from the University of Maine. SDCNF powders were produced by spray drying 1.2 wt % of the CNF suspension on a pilot-scale spray dryer (GEA-Niro, Columbia, MD, USA). The spray drying processed parameters were an inlet temperature of 250 °C, a disk spinning rate of 30,000 rpm and a feeding rate of 0.4 L/min.

2.2. Composite Manufacturing

A masterbatch was used to manufacture the SDCNF-reinforced iPP composites. More masterbatch manufacturing details are available elsewhere [15]. Raw materials were oven-dried for 2 h at 105 °C. SDCNF and iPP were hand-mixed using a fiber content of 30 wt % and metered into a co-rotating twin-screw extruder (C. W. Brabender Instruments, South Hackensack, NJ, USA) for compounding. The extruder process parameters were 200 °C across the heating sections with an extrusion speed of 250 rpm. Cooled extrudates were ground using a granulator (Hellweg MDS 120/150, Hackensack, NJ, USA) to obtain masterbatch pellets. The masterbatch pellets, fresh iPP and MAPP were mixed and compounded to make pellets containing 3 wt %, 10 wt % and 30 wt % SDCNF with and without MAPP. The oven-dried compounded pellet formulations were injection molded using a Model #50 "Minijector" at an injection pressure of 17 MPa and temperature of 200 °C. As-received iPP experienced exactly same processing history to be served as a control. The formulations of the iPP/SDCNF composites are listed in Table 2.

Table 2. Formulations of iPP/spray-dried cellulose nanofibrils (SDCNF) composites.

Samples	Labels	iPP (wt %)	SDCNF (wt %)	MAPP (wt %)
iPP	iPP	100	0	0
iPP + MAPP	iPP/MA	98	0	2
iPP + 3% SDCNF	iPP/SDCNF3%	97	3	0
iPP + MAPP + 3% SDCNF	iPP/MA/SDCNF3%	95	3	2
iPP + 10% SDCNF	iPP/SDCNF10%	90	10	0
iPP + MAPP + 10% SDCNF	iPP/MA/SDCNF10%	88	10	2
iPP + 30% SDCNF	iPP/SDCNF30%	70	30	0
iPP + MAPP + 30% SDCNF	iPP/MA/SDCNF30%	68	30	2

2.3. Nonisothermal Crystallization Study

Nonisothermal crystallization behavior of the composites was determined using a differential scanning calorimeter (DSC) (Instruments Q 2000, New Castle, DE, USA). About 1–2 mg of samples were obtained from the pellets and sealed in T_{zero} aluminum pans. The weight was selected to ensure that the pan lid was not broken during the pan sealing procedure. Samples were heated to 190 °C at a heating rate of 50 °C/min and held at that temperature for 5 min to erase thermal history. Four cooling rates (5, 10, 15 and 20 °C/min) were used examined for the crystallization study. Samples were cooled down to 50 °C and their crystallization curves recorded. A cooling rate of 20 °C/min is the fastest cooling rate the DSC achieves when the temperature is 50 °C. Samples were then reheated from 50 °C to 190 °C at a temperature ramp of 10 °C/min to measure melting behavior. All DSC measurements were performed in a nitrogen atmosphere at a flow rate of 50 mL/min. The crystallinity of iPP in the composites was calculated based on the following equation:

$$X_c = \Delta H_m / \left(\Delta H_f^0 \times \Phi \right) \quad (1)$$

where ΔH_m is melting enthalpy of iPP, ΔH_f^0 is the fusion enthalpies of iPP with 100% crystallinity and was reported to be 209 J/g from the literature [4]. The Φ is the fraction of the polymer contained in the composites. A new sample was used for each cooling rate.

2.4. Microscopy Study

The crystal morphology of iPP/SDCNF composites was measured using a ME520 Series polarized light microscope (PLM) (AmScope, Irvine, CA, USA). Sections of 3 µm-thick were acquired from the cross section of injection molded specimens using a Sorvall MT2-B Ultramicrotome. Each microtomed section was placed between a glass slide and a cover slip then transferred to a heating plate (Thermo Scientific, Waltham, MA, USA) operated at 200 °C. The microtomed section remained on the hot plate for 2 min before it was set aside and cooled to room temperature. It was observed that after 2 min of heat exposure, sections were partially melted, generating images with better quality [14]. To visualize the distribution of SDCNF in iPP, a scanning electron microscope (SEM) was used and (Hitachi High-Technologies Corporation, Tokyo, Japan). The cross sections of impact fractured specimens were directly observed using this SEM at an accelerating voltage of 15 KV.

2.5. Coefficient of Thermal Expansion (CTE)

Coefficient of thermal expansion measurements were conducted on the injection-molded specimens along the flow direction according to ASTM D 696-16. Because iPP has a glass transition temperature around 0 °C, thermal expansion measurements were performed separately over a temperature range from −30 °C to 30 °C. The thermal expansion above T_g of iPP is larger than that below T_g. For this study, the thermal expansion above T_g is of greater interest. The equation used to calculate the coefficient of thermal expansion is

$$\alpha = \Delta L / L_0 \Delta T \quad (2)$$

where ΔL is the change in length of specimen caused by temperature change, L_0 is the length of specimen at room temperature and ΔT is the change in temperature which is 30 °C. Three replicates were measured for the CTE measurements.

3. Results and Discussion

3.1. Nonisothermal Crystallization Kinetics

The crystallization kinetics of iPP and its composites are displayed in Table 3. As a basic trend, the onset temperature (T_o), crystallization peak temperature (T_p) and crystallinity of iPP (X_c) of all

samples decreased as the cooling rate increased. At a slower cooling rate, more crystal nuclei can be activated in the same time interval. Therefore, the crystallization occurs more completely during slow cooling than fast cooling [18]. No consistent trend in the change of T_o and T_p was caused by the addition of SDCNF at different fiber contents. The increase in X_c induced by the SDCNF is slight except at 30 wt % loading level (up to 19%). This indicates that SDCNF is a weak nucleation agent for iPP at low fiber content. The nucleation ability of natural fibers in a polymer matrix depends on factors like fiber size, chemical composition, surface polarity and surface topography where the surface topography is a decisive factor [24]. A coarse fiber is a better heterogeneous nucleation agent. Based on a previous study, SDCNF is mostly a spherical particle with a smooth surface [14,15]. This explains the weak nucleation ability of SDCNF for iPP and makes the SDCNF a suitable additive for iPP targeting EAM processing.

Table 3. Nonisothermal crystallization parameters at various cooling rates.

Samples	λ [a] (K/min)	T_o [b] (°C)	T_p [c] (°C)	X_c [d] (%)	$t_{1/2}$ [e] (min)
iPP	5	134.8	126.1	49.0	1.75
	10	131.2	122.7	49.6	0.88
	15	129.2	120.8	48.4	0.59
	20	127.2	119.0	46.1	0.46
iPP/SDCNF3%	5	134.0	125.9	50.0	1.59
	10	131.8	122.6	48.4	0.85
	15	129.7	120.9	45.9	0.60
	20	127.5	118.7	47.8	0.47
iPP/SDCNF10%	5	135.2	125.8	51.6	1.85
	10	131.8	122.6	48.2	0.95
	15	130.4	120.7	49.3	0.66
	20	128.9	119.5	49.1	0.49
iPP/SDCNF30%	5	134.3	126.2	56.4	1.56
	10	132.3	123.2	54	0.88
	15	130.3	121.3	57.6	0.58
	20	128.7	120.2	47.7	0.42
iPP/MA	5	133.4	125.8	53.4	1.51
	10	130.9	122.8	51.9	0.81
	15	129.4	121.0	49.3	0.56
	20	127.2	119.3	47.1	0.41
iPP/MA/SDCNF10%	5	133.0	125.3	52.1	1.51
	10	130.8	122.4	50.1	0.83
	15	128.6	120.3	49.2	0.55
	20	127.1	118.3	49.3	0.46

[a] λ—cooling rate; [b] T_o—onset temperature; [c] T_p—peak temperature; [d] X_c—crystallinity and [e] $t_{1/2}$—half crystallization time.

During nonisothermal crystallization, the relative degree of crystallinity (X_t) is a function of crystallization temperature that can be calculated from the following equation [25]:

$$X_t = \int_{T_0}^{T} (\frac{dH_c}{dT})dT / \int_{T_0}^{T_\infty} (\frac{dH_c}{dT})dT \quad (3)$$

where T_o is the onset temperature, T is the temperature at time t, T_∞ is the temperature when crystallization completes, dH_c is the enthalpy of crystallization. The X_t can also be associated with the crystallization time considering the conversion from T to t:

$$t = (T_o - T)/\lambda \quad (4)$$

where λ is the cooling rate.

In Table 3, the $t_{1/2}$ refers to the time when 50% X_t was achieved. As cooling rate increases, the $t_{1/2}$ decreases. This trend is consistent with previous study on iPP and natural fiber-filled iPP composites [18,26]. With the incorporation of SDCNF at 3 wt %, the $t_{1/2}$ of iPP decreased by 9% at λ = 5 K/min. At 30 wt % SDCNF content, the $t_{1/2}$ of iPP was reduced by 11% at λ = 5 K/min. SDCNF at those loading levels accelerated the crystallization rate of iPP. However, at 10 wt % loading level of SDCNF, the $t_{1/2}$ of iPP was lowered by 6%, indicating SDCNF retarded the crystallization rate of iPP. The addition of MAPP into iPP/SDCNF composite increased the crystallization rate of iPP by 14% at λ = 5 K/min. There are three possible reasons. First, MAPP alone is reported to be a nucleating agent for iPP that helps to form more spherulitic sites and smaller spherulites [5]. This is confirmed by the shorter $t_{1/2}$ of iPP/MA composites in Table 3. Second, MAPP was found to increase the equilibrium melting point of wood flour/PP composites thus enlarging the degree of undercooling for the system by facilitating the chain relaxation at the interfaces [24]. A higher degree of undercooling is directly associated with faster crystallization. Lastly, MAPP can improve the compatibility between SDCNF and iPP, distributing SDCNF better in iPP and thus enhancing the nucleation ability of SDCNF. Therefore, MAPP is not necessarily an appealing additive for EAM processing of iPP. The overall crystallization rate of iPP depends on the nucleation rate and crystal growth rate [27]. The addition of SDCNF at various loading levels increases the nucleation rate and retards crystal growth rate at various degrees, yielding the observed results. Microscopy of the crystal structure can help explain these results and will be discussed in a subsequent section. To help understand how the crystallization kinetics behaved, in the next section, nonisothermal crystallization kinetic models were applied to fit the experimental data.

3.2. Nonisothermal Crystallization Kinetics Modeling

3.2.1. Jeziorny Method

Both isothermal and nonisothermal crystallization processes can be described by the Avrami's model [26]. The relation between relative degree of crystallinity (X_t) and elapsed crystallization time (t) is as follows:

$$1 - X_t = \exp(-Kt^n) \tag{5}$$

where K is the kinetic constant related to nucleation and crystal growth and n is the Avrami exponent that is determined by the geometry of the nucleated and grew crystals. The higher the K, the faster the crystallization rate. In practice, the above equation is expressed in its double logarithmic form:

$$\ln\left[-\ln(1 - X_t)\right] = n \ln\ t + \ln\ K \tag{6}$$

Plot $\ln[-\ln(1 - X_t)]$ against $\ln t$ within the X_t range of (0.01~63%) yields a straight line (Figure 2). At higher X_t, curves lose linearity because secondary crystallization and impingement of crystals dominate the process, which makes the Avrami's method inapplicable [28,29]. The slope of the line is n and the intercept with the y axis is $\ln K$. Because the crystallization temperature changes during nonisothermal crystallization, n and K are merely curve-fitting parameters with no physical meaning [26]. Modification of the Avrami's model was made by Jeziorny to make it meaningful to describe the nonisothermal crystallization kinetics [30]. The parameter K was corrected to consider the effect of cooling rate during the test. The modified crystallization rate constant K_J was calculated by

$$\ln\ K_J = (\ln\ K)/\lambda \tag{7}$$

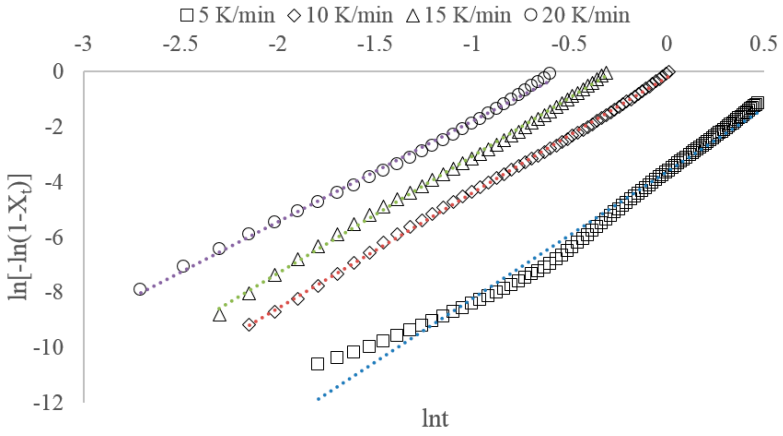

Figure 2. Plot of $\ln[-\ln(1 - X_t)]$ against $\ln t$ of iPP/SDCNF10% composites according to Jeziorny model during crystallization at various cooling rates.

Data from fitting the curves obtained from Jeziorny method are displayed in Table 4. Generally, n decreases and K_J increases as cooling rate increases. For iPP, n varied from 4.57 to 5.33, indicative of tridimensional crystal growth [17]. Similar n values were reported by previous research on natural fiber filled PP [16–18]. After the SDCNF was added to the polymer, n decreases. This is because SDCNF, being a nucleating agent, generates more heterogeneous nucleation [16]. The iPP/SDCNF3%, iPP/SDCNF30% and iPP/MA/SDCNF10% have larger K_J than iPP at a slower cooling rate. This is consistent with the $t_{1/2}$ values in Table 3. A similar change in the K_J of iPP caused by the addition of microcrystalline cellulose was reported [17]. The iPP/SDCNF10% has a smaller K_J than iPP, which is consistent with the results in Table 3. Therefore, the Jeziorny method is effective in describing the nonisothermal crystallization kinetics of iPP/SDCNF composites.

Table 4. Crystallization parameters calculated from Jeziorny method.

Samples	λ [a]	n	K_J	R^2
iPP	5	5.33	0.49	0.991
	10	4.89	0.99	0.998
	15	4.60	1.11	0.999
	20	4.57	1.13	0.997
iPP/SDCNF3%	5	4.33	0.58	0.983
	10	5.07	1.02	0.999
	15	4.30	1.10	0.998
	20	3.66	1.10	0.995
iPP/SDCNF10%	5	5.19	0.48	0.997
	10	3.98	0.98	0.999
	15	4.23	1.08	0.999
	20	3.65	1.10	0.997
iPP/SDCNF30%	5	4.26	0.62	0.995
	10	4.41	1.00	0.999
	15	3.75	1.09	0.999
	20	3.16	1.11	0.997
iPP/MA/SDCNF10%	5	4.23	0.61	0.984
	10	4.69	1.03	0.999
	15	3.98	1.11	0.998
	20	3.90	1.12	0.999

[a] λ—cooling rate.

3.2.2. Ozawa Method

The Ozawa method considers the nonisothermal crystallization process as a sum of many isothermal crystallization processes occurring at an infinitesimal time over the crystallization period [31]. His mathematical model was also based on the Avrami equation:

$$1 - X_t = \exp[-K(T)/\lambda^m] \tag{8}$$

where $K(T)$ is the crystallization constant, depending on the crystallization temperature. And m is the Ozawa exponent. A double logarithmic form can also be converted from above equation:

$$\ln[-\ln(1 - X_t)] = \ln K(T) - m \ln(\lambda) \tag{9}$$

A plot of $\ln[-\ln(1 - X_t)]$ versus $\ln \lambda$ at different crystallization temperatures should result in linear curves (Figure 3). Then $K(T)$ and m can be obtained from the intersection and slope. As seen from the Ozawa graphs, the curves are relatively linear at lower crystallization temperature. At high crystallization temperature, the curves deviate far from linearity. The Ozawa method does not consider the secondary crystallization which can occur at the early stage during the crystallization [16]. Therefore, the Ozawa method is not effective in describing the nonisothermal crystallization of iPP/SDCNF composites. This conclusion is consistent with previous findings [16–18]. No additional analysis was performed using this method.

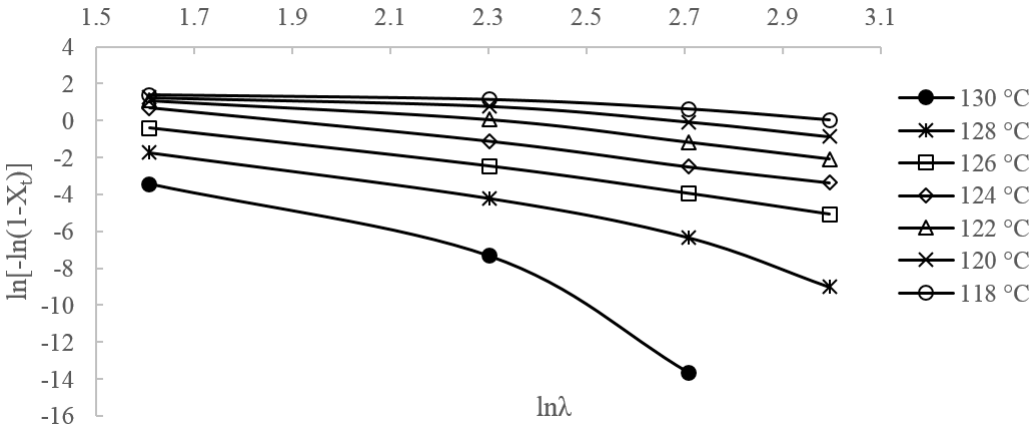

Figure 3. Plots of $\ln[-\ln(1 - X_t)]$ as a function of $\ln \lambda$ for iPP/SDCNF10% composites based on Ozawa method.

3.2.3. Liu Method

Liu et al. proposed a method to exactly describe the nonisothermal crystallization kinetics by combining Avrami and Ozawa methods [32]. The equation is

$$\ln \lambda = \ln F(T) - \alpha \ln t \tag{10}$$

$$F(T) = [K(T)/K]^{1/m} \tag{11}$$

$$\alpha = n/m \tag{12}$$

where $F(T)$ is the degree of cooling rate required during unit crystallization time when the polymer has a certain degree of crystallinity. The smaller the $F(T)$, the faster the crystallization. K is the Avrami constant, n is the Avrami exponent, $K(T)$ is the Ozawa constant, m is the Ozawa exponent and λ is the cooling rate. Plotting $\ln \lambda$ against $\ln t$ results in a linear curve as shown in Figure 4. The α and $\ln F(T)$ can be achieved from the slope and intercept of these curves. Kinetic parameters from the Liu method

are shown in Table 5. The α values of iPP and iPP/SDCNF are close to 1, meaning the Jezioney and Ozawa methods are similar in modeling the nucleation mechanism and crystal geometry, especially at low X_t. The $F(T)$ increases monotonically with the increase of X_t, indicating that crystallization becomes more difficult at higher X_t. The iPP/SDCNF3%, iPP/SDCNF30% and iPP/MA/SDCNF10% slightly decreases $F(T)$ of iPP when compared at the same X_t, meaning that SDCNF at these loading levels accelerates the crystallization rate of iPP. The iPP/SDCNF10% has the opposite effect on $F(T)$ of iPP compared to the other loading levels, meaning SDCNF10% retards the iPP crystallization rate. These findings are consistent with the information provided by $t_{1/2}$ in Table 3. Therefore, the Liu method is effective in describing the nonisothermal crystallization kinetics of SDCNF/iPP composites.

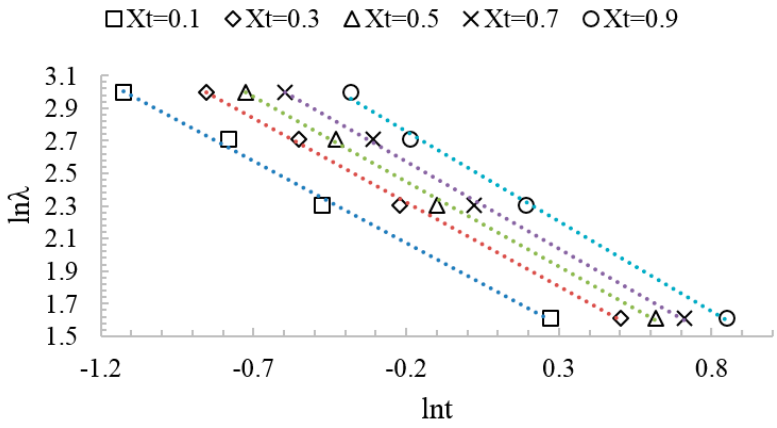

Figure 4. Plots of ln λ as a function of ln t at different X_t for iPP/SDCNF10% composites based on the Liu method.

Table 5. Crystallization parameters calculated from Liu method.

Sample	X_t [a] (%)	α	$F(T)$	R^2
iPP	10	0.95	6.50	0.999
	30	1.00	7.86	0.999
	50	1.03	8.85	0.999
	70	1.07	9.95	0.999
	90	1.16	12.38	0.998
iPP/SDCNF3%	10	1.10	5.80	0.999
	30	1.11	7.47	0.999
	50	1.14	8.46	1.000
	70	1.20	9.65	0.999
	90	1.29	11.97	0.994
iPP/SDCNF10%	10	1.01	6.51	0.996
	30	1.03	8.28	0.998
	50	1.04	9.38	0.998
	70	1.07	10.57	0.999
	90	1.11	12.62	0.997
iPP/SDCNF30%	10	1.00	5.52	0.988
	30	1.05	7.22	0.995
	50	1.07	8.33	0.995
	70	1.10	9.45	0.997
	90	1.14	11.53	0.997
iPP/MA/SDCNF10%	10	1.08	5.45	0.996
	30	1.12	7.00	0.999
	50	1.15	8.05	0.996
	70	1.18	9.13	0.993
	90	1.27	11.35	0.994

[a] X_t—relative degree of crystallinity.

3.2.4. Effective Activation Energy

The effective activation energy (ΔE) during polymer crystallization refers to the energy required to transport macromolecular segments to the surface of a crystal [18]. The Kissinger equation has been used to calculate ΔE using crystallization peak temperature (T_p) and cooling rate (λ) [33]. The Kissinger method equation is:

$$d\left[\ln\left(\lambda/T_p^2\right)\right] = -\frac{\Delta E}{R}d\left(1/T_p\right) \quad (13)$$

where λ is the cooling rate, T_p is the peak crystallization temperature and R is the universal gas constant (8.314 J/(K*mol)). Plotting ln (λ/T_p^2) against $1/T_p$ yields a linear curve as in Figure 5. ΔE can be obtained from the slope. Activation energies of different samples are listed in Table 6. These activation energy values are close to what were reported for natural fiber-filled iPP [18]. The ΔE of iPP/SDCNF3% is similar to iPP. On the other hand, iPP/SDCNF10% and iPP/SDCNF30% increase the ΔE of iPP. The SDCNF at 30 wt % appears more likely to retard the crystallization speed of iPP. Moreover, adding MAPP into iPP/SDCNF10% largely reduced the ΔE. These seemingly conflicting results can be explained by considering the two components that determine the overall crystallization rate and transcrystallization phenomenon which are analyzed in next section.

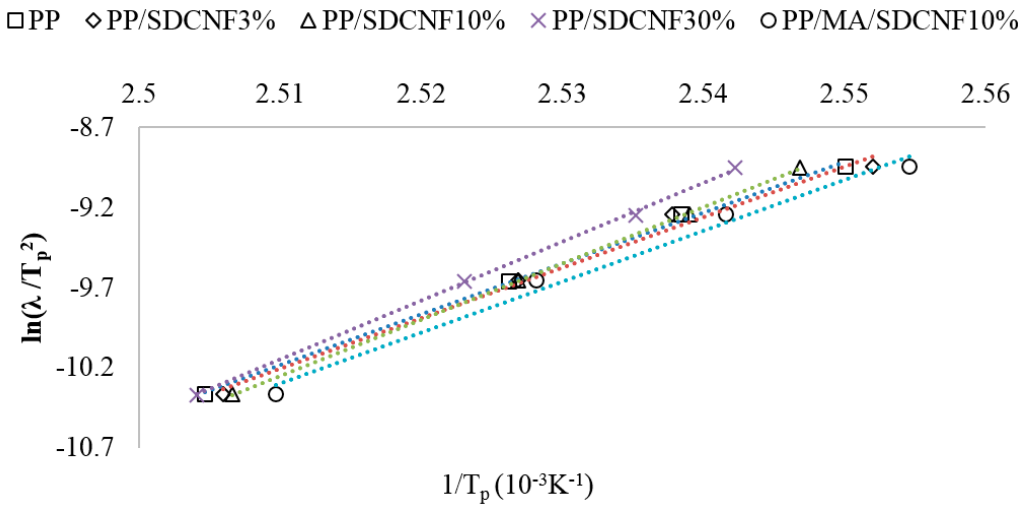

Figure 5. Plot of ln (λ/T_p^2) against $1/T_p$ for obtaining ΔE based on Kissinger method.

Table 6. Effective activation energy calculated based on the Kissinger method.

Samples	iPP	iPPSDCNF3%	iPPSDCNF10%	iPPSDCNF30%	iPP/MA/SDCNF10%
ΔE (kJ/mol)	264.1	262.5	291.6	305.5	265.2
R^2	0.997	0.989	0.999	0.999	0.988

It is worthy to note that besides using traditional models to fit the DSC data, researchers have developed simulation tools using finite element analysis to predict the crystallization kinetics of semi-crystalline thermoplastics [10]. The simulation provided reasonable results without time-consuming analysis with experiments.

3.3. Microscopy Study

As seen in Figure 6, the distribution of SDCNF within the iPP is relatively good up to 30 wt % fiber content. However, the dispersion of individual CNF was not achieved because the shear forces during compounding did not break down the SDCNF agglomerates [15]. The space among SDCNF in iPP/SDCNF3% is large. As the SDCNF content increases, the space among SDCNF becomes smaller.

At 30 wt % level, the gaps among SDCNF are the smallest. When more SDCNF is added into iPP, the free volume of iPP is reduced, imposing restriction on the crystallization of iPP.

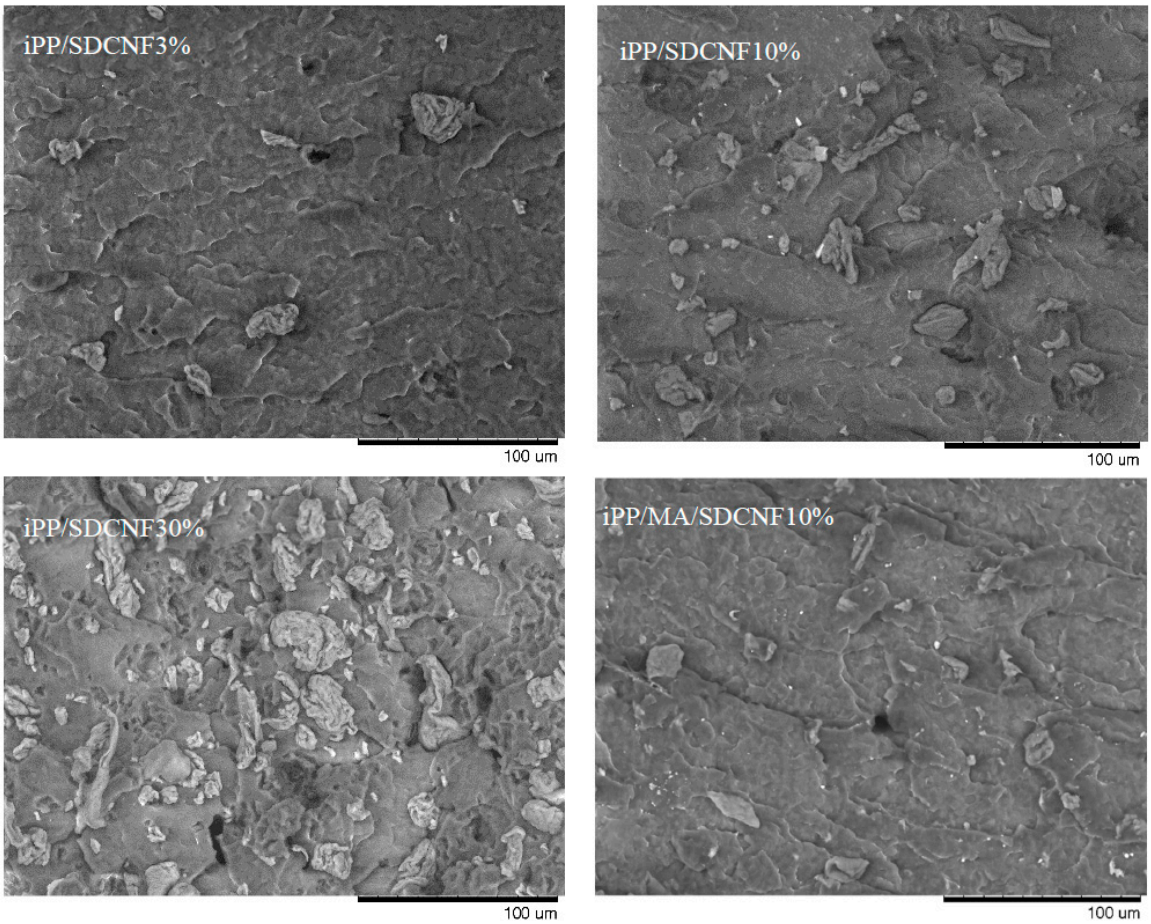

Figure 6. SEM micrographs showing the distribution of SDCNF within iPP.

Injection-molded iPP and iPP/SDCNF composites were used as examples to illustrate the effect of SDCNF on the crystalline morphology of iPP by polarized light microscopy as shown in Figure 7. Because no cold-crystallization peaks were observed in the DSC scans for all specimens, the crystalline morphology caused by microtome preparation of the samples was negligible [14]. As SDCNF content increases, nucleation density increases, as indicated by the number of spherulites within the same area. For example, in iPP/SDCNF3% (left bottom), one long SDCNF nucleates several iPP spherulites on its surface. Meanwhile, spherulite's size decreases as SDCNF content increases. Crystal diameters of iPP, iPP/MA, iPP/SDCNF3%, iPP/SDCNF10%, iPP/SDCNF30% and iPP/MA/SDCNF10% are 30 ± 3 µm, 27 ± 2 µm, 29 ± 2 µm, 19 ± 2 µm, 11 ± 2 µm and 16 ± 3 µm. A previous study on the isothermal crystallization kinetics of cellulose nanocrystals (CNC)-filled PP found that adding 1 wt % spray-freeze-dried CNC increased the chain-folding work of PP significantly [29]. This implies that the CNC restricted the folding motion of polymer chains during crystallization and made the re-entry of polymer chains into the crystal face more difficult, resulting in smaller crystals [29]. Similar results were reported for polymer composites containing a high content of nanofillers [11–13]. Hence, steric hindrance attributed to the large amount of SDCNF is the reason for the higher ΔE for iPP as shown in Table 6. As a compatibilizer, MAPP helps PP to wet the natural fiber better [24]. Also, MAPP is reported to facilitate transcrystallization, a process where spherulites grow perpendicularly to the surface [34]. Transcrystallization provides additional sites and directions for crystals to grow, thus reducing the ΔE. A possible site of SDCNF transcrystallization was identified for iPP/MA/SDCNF10%

in Figure 7 (right bottom). As a comparison, the morphology of iPP spherulites on SDCNF surface in iPP/SDCNF3% composite is also shown which has no transcrystallization (bottom left). This may prove the role of MAPP in transcrystalline layer formation.

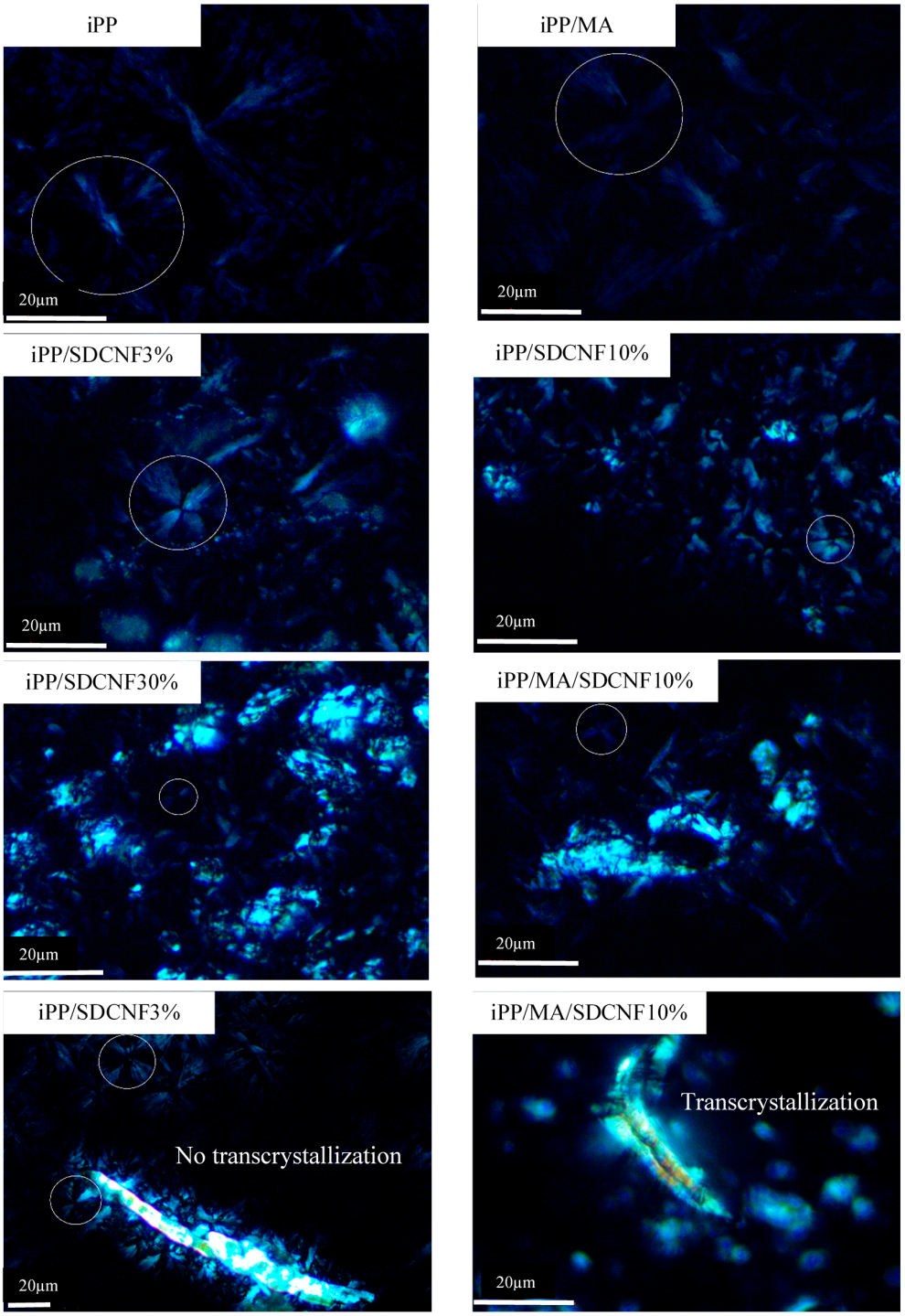

Figure 7. Polarized light micrographs of iPP and iPP/SDCNF composites. Bright and irregular-shape clumps are SDCNF. Inside the circles are the Maltese-cross patterns of iPP spherulites. The last two graphs show the effect of maleic anhydride polypropylene (MAPP) on transcrystallization using different scale bars.

The overall crystallization rate of a polymer depends on both nucleation rate and crystal growth rate [27]. The addition of SDCNF increased the nucleation rate by providing heterogeneous nucleation sites. Meanwhile, crystal growth rate was impeded by the SDCNF attributed to steric hindrance and reduced free volume. At 10 wt % addition of SDCNF, the increase in nucleation rate was outweighed by the decrease in crystal growth rate. Therefore, only iPP/SDCNF10% showed slower crystallization rate than iPP in this study.

3.4. Thermal Expansion

Based on the results from nonisothermal crystallization kinetics study, SDCNF at 10 wt % without MAPP was selected to be incorporated into iPP for EAM. The effect of SDCNF on the thermal expansion of iPP was investigated and the results are listed in Table 7. The CTE of iPP is within the CTE range of iPP reported by previous research [35,36]. After adding 10 wt % SDCNF into the iPP, the CTE decreased by 11.7%. This change is comparable with a previous study where the CTE of iPP containing 10 wt % wood flour was reduced by 16.9%. Because cellulose possesses a small CTE and the addition of SDCNF replaces a portion of iPP, the composite displays a smaller CTE [23]. This would help reduce the iPP shrinkage caused by temperature changes below the crystallization temperature during the EAM.

Table 7. Coefficient of thermal expansion of iPP and iPP/SDCNF composites.

Samples	α [a] (10^{-6}/°C)	Significance
iPP	80.1 (3.1) [b]	A [c]
iPP/SDCNF10%	70.7 (2.4)	B

[a] coefficient of thermal expansion; [b] standard deviation and [c] capital letters represent statistical differences. Values with different letters are significantly different at 95% confidence level.

4. Conclusions

This study investigated the SDCNF content and the use of MAPP on the nonisothermal crystallization kinetics of SDCNF reinforced iPP composites. The iPP/SDCNF3% and iPP/SDCNF30% reduced the $t_{1/2}$ of iPP. This implied that SDCNF at these two levels accelerated iPP's crystallization rate. In contrast, iPP/SDCNF10% increased the $t_{1/2}$ of iPP, retarding iPP's crystallization rate. The addition of MAPP into iPP/SDCNF10% composites reduced the $t_{1/2}$ of iPP. This is because MAPP is a nucleating agent and can facilitate transcrystallization. The Jeziorny and Liu methods were proven to be valid in describing the nonisothermal crystallization process of iPP reinforced by SDCNF where the Ozawa method did not work. The ΔE of iPP, calculated based on Kissinger method, was similar to that of iPP/SDCNF3%, but smaller than those of iPP/SDCNF10% and iPP/SDCNF30%. The existence of SDCNF at high loading level restricts the diffusion and folding of polymer chains during crystallization by reducing the free volume of iPP. The addition of MAPP into iPP/SDCNF10% lowered the ΔE because MAPP facilitated the occurrence of transcrystallization. The PLM graphs further confirmed that a large amount of SDCNF can impede the crystal growth of iPP. Generally, the nucleation rate was increased by the addition of SDCNF. At 10 wt % SDCNF, the increase in nucleation rate was outweighed by the decreased crystal growth rate, making SDCNF a crystallization rate retardant. Moreover, the CTE of iPP/SDCNF10% composites was 11.7% smaller than iPP. Based on this study, SDCNF at 10 wt % loading level can help to reduce the shrinkage iPP caused by temperature changes during EAM processing.

Acknowledgments: Funding is provided in part by the Maine Agricultural and Forest Experiment Station (MAFES) project ME0-M-8-00527-13 and the USDA ARS Forest Products Research Agreement 58-0202-4-003. Authors thank Kelly Edwards in the Electron Microscopy Lab for microscopic section preparation.

Author Contributions: Lu Wang and Douglas J. Gardner conceived and designed the experiments; Lu Wang performed the experiments; Lu Wang analyzed the data and wrote the paper; Douglas J. Gardner, William M. Gramlich, Yousoo Han and Mehdi Tajvidi revised the manuscript. All authors approved the final version of the paper.

Conflicts of Interest: The authors declare no conflict of interest.

References

1. Wang, L.; Sanders, J.E.; Gardner, D.G.; Han, Y. In-situ modification of cellulose nanofibrils by organosilanes during spray drying. *Ind. Crops Prod.* **2016**, *93*, 129–135. [CrossRef]
2. Siqueira, G.; Bras, J.; Dufresne, A. Cellulose whiskers versus microfibrils: Influence of the nature of the nanoparticle and its surface functionalization on the thermal and mechanical properties of nanocomposites. *Biomacromolecules* **2008**, *10*, 425–432. [CrossRef] [PubMed]
3. Peng, Y.; Gardner, D.J.; Han, Y. Drying cellulose nanofibrils: In search of a suitable method. *Cellulose* **2012**, *19*, 91–102. [CrossRef]
4. Wang, L.; Gardner, D.J. Effect of fused layer modeling (FLM) processing parameters on impact strength of cellular polypropylene. *Polymer* **2017**, *113*, 74–80. [CrossRef]
5. Seo, Y.; Kim, J.; Kim, K.U.; Kim, Y.C. Study of the crystallization behaviors of polypropylene and maleic anhydride grafted polypropylene. *Polymer* **2000**, *41*, 2639–2646. [CrossRef]
6. Fujisawa, S.; Zhang, J.; Saito, T.; Iwata, T.; Isogai, A. Cellulose nanofibrils as templates for the design of poly(L-lactide)-nucleating surfaces. *Polymer* **2014**, *55*, 2937–2942. [CrossRef]
7. Sun, Q.; Rizvi, G.M.; Bellehumeur, C.T.; Gu, P. Effect of processing conditions on the bonding quality of FDM polymer filaments. *Rapid Prototyp. J.* **2008**, *14*, 72–80. [CrossRef]
8. Le Bozec, Y.; Kaang, S.; Hine, P.J.; Ward, I.M. The thermal-expansion behavior of hot-compacted polypropylene and polyethylene composites. *Compos. Sci. Technol.* **2000**, *60*, 333–344. [CrossRef]
9. Ratajski, E.; Janeschitz-Kriegl, H. Flow-induced crystallization in polymer melts: On the correlation between nucleation and specific work. *Polym. Bull.* **2012**, *68*, 1723–1730. [CrossRef]
10. Spina, R.; Spekowius, M.; Hopmann, C. Multiphysics simulation of thermoplastic polymer crystallization. *Mater. Des.* **2016**, *95*, 455–469. [CrossRef]
11. Fornes, T.D.; Paul, D.R. Crystallization behavior of nylon 6 nanocomposites. *Polymer* **2003**, *44*, 3945–3961. [CrossRef]
12. Li, L.; Li, C.Y.; Ni, C.; Rong, L.; Hsiao, B. Structure and crystallization behavior of Nylon 66/multi-walled carbon nanotube nanocomposites at low carbon nanotube contents. *Polymer* **2007**, *48*, 3452–3460. [CrossRef]
13. Deshmukh, G.S.; Peshwe, D.R.; Pathak, S.U.; Ekhe, J.D. Nonisothermal crystallization kinetics and melting behavior of poly (butylene terephthalate) and calcium carbonate nanocomposites. *Thermochim. Acta* **2015**, *606*, 66–76. [CrossRef]
14. Wang, L.; Roach, A.W.; Gardner, D.J.; Han, Y. Mechanisms contributing to mechanical property changes in composites of polypropylene reinforced with spray-dried cellulose nanofibrils. *Cellulose* **2018**, *25*, 439–448. [CrossRef]
15. Wang, L.; Gardner, D.J.; Bousfield, D.W. Cellulose nanofibril-reinforced polypropylene composites for material extrusion: Rheological properties. *Polym. Eng. Sci.* **2017**. [CrossRef]
16. Grozdanov, A.; Buzarovska, A.; Bogoeva-Gaceva, G.; Avella, M.; Errico, M.E.; Gentile, G. Nonisothermal crystallization kinetics of kenaf fiber/polypropylene composites. *Polym. Eng. Sci.* **2007**, *47*, 745–749. [CrossRef]
17. Zhu, X.L.; Wang, C.S.; Wang, B.; Wang, H.P. Non-isothermal crystallization kinetics and nucleation activity of filler in polypropylene/microcrystalline cellulose composites. *Iran. Polym. J.* **2008**, *17*, 297–309.
18. Phuong, N.T.; Gilbert, V. Non-isothermal crystallization kinetics of short bamboo fiber-reinforced recycled polypropylene composites. *J. Reinf. Plast. Compos.* **2010**, *29*, 2576–2591. [CrossRef]
19. Xu, N.; Xue, F.; Ding, E. Nonisothermal crystallization kinetics in isotactic polypropylene/microcrystalline cellulose (II) composites. *Polym. Compos.* **2016**. [CrossRef]

20. Quillin, D.T.; Yin, M.; Koutsky, J.A.; Caulfield, D.F. Crystallinity in the polypropylene/cellulose system. II. Crystallization kinetics. *J. Appl. Polym. Sci.* **1994**, *52*, 605–615. [CrossRef]
21. Janicek, M.; Polaskova, M.; Holubar, R.; Cermak, R. Surface-esterified cellulose fiber in a polypropylene matrix: Impact of esterification on crystallization kinetics and dispersion. *Cellulose* **2014**, *21*, 4039–4048. [CrossRef]
22. Ito, H.; Hattori, H.; Okamoto, T.; Takatani, M. Thermal expansion of high filler content cellulose-plastic composites. *J. Wood Chem. Technol.* **2010**, *30*, 360–372. [CrossRef]
23. Huang, R.; Zhang, Y.; Xu, X.; Zhou, D.; Wu, Q. Effect of hybrid mineral and bamboo fillers on thermal expansion behavior of bamboo fiber and recycled polypropylene–polyethylene composites. *BioResources* **2012**, *7*, 4563–4574. [CrossRef]
24. Wang, P.; Liu, J.; Yu, W.; Zhou, C. Isothermal crystallization kinetics of highly filled wood plastic composites: Effect of wood particles content and compatibilizer. *J. Macromol. Sci. B* **2011**, *50*, 2271–2289. [CrossRef]
25. Herrero, C.R.; Acosta, J.L. Effect of poly (epichlorhydrin) on the crystallization and compatibility behavior of poly (ethylene oxide)/polyphosphazene blends. *Polym. J.* **1994**, *26*, 786–796. [CrossRef]
26. Ou, R.; Guo, C.; Xie, Y.; Wang, Q. Non-isothermal crystallization kinetics of Kevlar fiber-reinforced wood flour/HDPE composites. *BioResources* **2011**, *6*, 4547–4565.
27. Hiemenz, P.C.; Lodge, T.P. Linear Viscosity. In *Polymer Chemistry*, 2nd ed.; CRC Press: Boca Raton, FL, USA, 2007; pp. 419–464.
28. Gopakumar, T.G.; Lee, J.A.; Kontopoulou, M.; Parent, J.S. Influence of clay exfoliation on the physical properties of montmorillonite/polyethylene composites. *Polymer* **2002**, *43*, 5483–5491. [CrossRef]
29. Khoshkava, V.; Ghasemi, H.; Kamal, M.R. Effect of cellulose nanocrystals (CNC) on isothermal crystallization kinetics of polypropylene. *Thermochim. Acta* **2015**, *608*, 30–39. [CrossRef]
30. Jeziorny, A. Parameters characterizing the kinetics of the non-isothermal crystallization of poly (ethylene terephthalate) determined by DSC. *Polymer* **1978**, *19*, 1142–1144. [CrossRef]
31. Ozawa, T. Kinetics of non-isothermal crystallization. *Polymer* **1971**, *12*, 150–158. [CrossRef]
32. Liu, T.; Mo, Z.; Wang, S.; Zhang, H. Nonisothermal melt and cold crystallization kinetics of poly (aryl ether ether ketone ketone). *Polym. Eng. Sci.* **1997**, *37*, 568–575. [CrossRef]
33. Kissinger, H.E. Variation of peak temperature with heating rate in differential thermal analysis. *J. Res. Natl. Bur. Stand.* **1956**, *57*, 217–221. [CrossRef]
34. Yin, S.; Rials, T.G.; Wolcott, M.P. Crystallization behavior of polypropylene and its effect on woodfiber composite properties. In Proceedings of the Fifth International Conference on Wood Fiber-Plastic Composites, Madison, WI, USA, 26–27 May 1999; pp. 139–146.
35. Yang, H.S.; Wolcott, M.P.; Kim, H.S.; Kim, H.J. Thermal properties of lignocellulosic filler-thermoplastic polymer bio-composites. *J. Therm. Anal. Calorim.* **2005**, *82*, 157–160. [CrossRef]
36. Kalaitzidou, K.; Fukushima, H.; Drzal, L.T. Multifunctional polypropylene composites produced by incorporation of exfoliated graphite nanoplatelets. *Carbon* **2007**, *45*, 1446–1452. [CrossRef]